

# Adaptive Spectral Feature Forecasting for Diffusion Sampling Acceleration

Jiaqi Han<sup>1†</sup> Juntong Shi<sup>1†</sup> Puheng Li<sup>1</sup> Haotian Ye<sup>1</sup> Qiushan Guo<sup>2</sup> Stefano Ermon<sup>1</sup>  
<sup>1</sup>Stanford University <sup>2</sup>ByteDance  
<https://hanjq17.github.io/Spectrum>

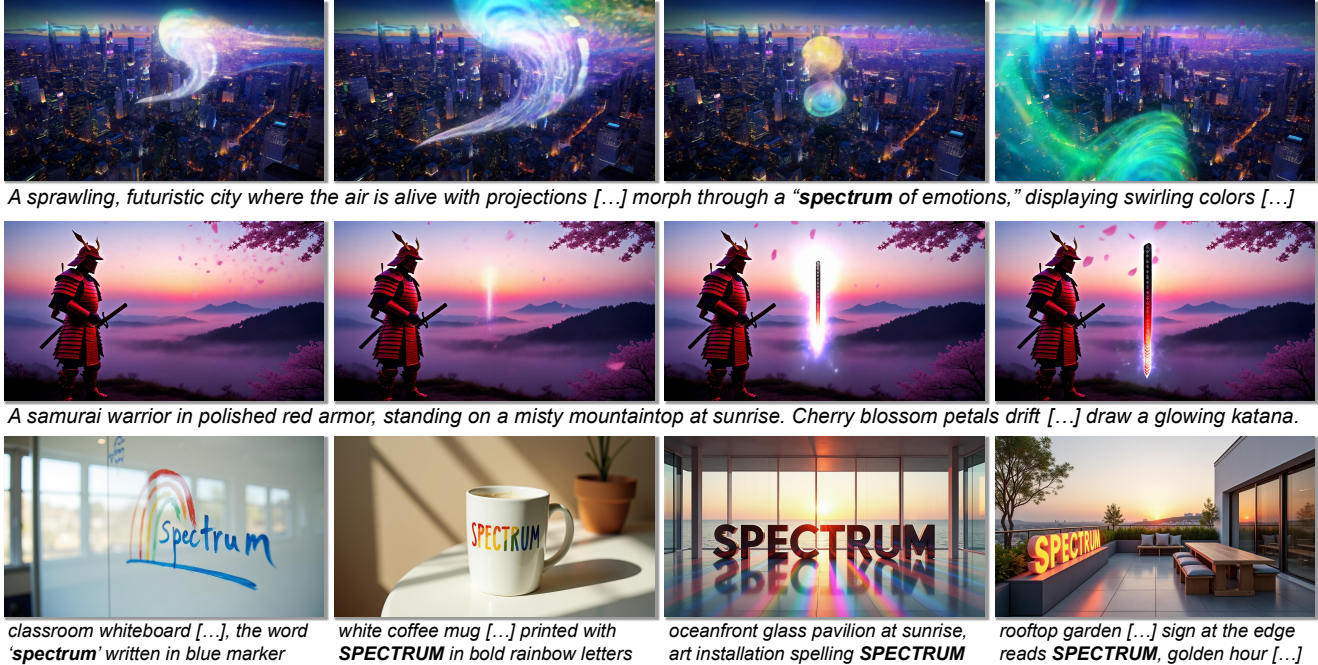


Figure 1. Text-to-video (top) and text-to-image (bottom) generated samples using our *Spectrum* on HunyuanVideo and FLUX.1, respectively. Samples were generated using only **14 network evaluations**, leading to a significant speedup of  $3.5\times$  without quality degradation.

## Abstract

Diffusion models have become the dominant tool for high-fidelity image and video generation, yet are critically bottlenecked by their inference speed due to the numerous iterative passes of Diffusion Transformers. To reduce the exhaustive compute, recent works resort to the feature caching and reusing scheme that skips network evaluations at selected diffusion steps by using cached features in previous steps. However, their preliminary design solely relies on local approximation, causing errors to grow rapidly with large skips and leading to degraded sample quality at high speedups. In this work, we propose spectral diffusion feature forecaster (Spectrum), a training-free approach that enables global, long-range feature reuse with tightly controlled error. In particular, we view the latent features of the denoiser as functions over time and approximate them with

Chebyshev polynomials. Specifically, we fit the coefficient for each basis via ridge regression, which is then leveraged to forecast features at multiple future diffusion steps. We theoretically reveal that our approach admits more favorable long-horizon behavior and yields an error bound that does not compound with the step size. Extensive experiments on various state-of-the-art image and video diffusion models consistently verify the superiority of our approach. Notably, we achieve up to  $4.79\times$  speedup on FLUX.1 and  $4.67\times$  speedup on Wan2.1-14B, while maintaining much higher sample quality compared with the baselines.

## 1. Introduction

Diffusion models have become the preeminent tool for high-fidelity image and video synthesis [4, 10, 34, 43, 46, 47, 53]. Their success, however, comes with a steep computational price: their sampling requires dozens to hundreds

<sup>†</sup>Equal. Correspondence to [jiaqihan@stanford.edu](mailto:jiaqihan@stanford.edu).

of evaluations of a large denoiser, which, for most state-of-the-art models, is typically a Diffusion Transformer [26, 32] with deep stacks of attention blocks. The dominant cost of inference poses practical limits for interactive applications that call for real-time model responses.

To address the challenge, various works have been proposed to reduce the sampling latency of diffusion models. Amongst them, feature caching-based approaches [21, 22, 30, 60, 61] have stood out and shown great promise in remarkably reducing the sampling time while maintaining desirable sample quality, all without additional training. Concretely, these methods cache latent features produced by certain blocks at selected timesteps and use them to synthesize features at future timesteps via light-weight predictors, thereby avoiding expensive denoiser evaluations. In particular, the naive copy strategy directly reuses the most recent cached feature [21, 40], while the recent work [22] performs discrete Taylor expansion using a few nearest cached points.

Despite their promise, through our error analysis and empirical verification, we find these *local* predictors incur approximation errors that compound rapidly as the forecasting horizon grows, leading to severe quality degradation at high speedup ratios. Furthermore, the local predictors, such as Taylor expansion, struggle to capture the long-range temporal dynamics of features along the sampling process, and are thus prone to producing images with inaccurate semantics. These limitations severely hinder their practical utility, particularly in high-speedup scenarios.

To this end, we move beyond local approximations and instead construct the forecaster in the *spectral* domain. Our key insight is to view each feature channel of the denoiser output along the diffusion trajectory as a function over time and approximate it with a compact set of global, orthonormal bases in function space. Notably, we leverage *Chebyshev polynomials* [33] to fit the functions via a ridge regression objective, motivated by their well-conditioned recurrences and favorable error behavior at long horizons [31]. The fitted coefficients are then employed to predict features at future steps, enabling large skips of actual network evaluations. The framework, which we coin *Spectral Diffusion Feature Forecaster (Spectrum)*, not only yields more tightly bounded error but also injects crucial long-range spectral semantics to the generated sample, substantially reducing the error and enhancing sample quality. With the benefits of such design, *Spectrum* produces image and video samples using only 14 network evaluations without quality degradation, as demonstrated in Fig. 1.

In summary, we make the following major contributions. **1.** We introduce spectral diffusion feature forecasting (*Spectrum*), the first feature caching-based diffusion acceleration approach that operates in the spectral domain. Critically, we leverage Chebyshev polynomials as the basis set due to its desirable properties for error reduction. **2.** We

perform thorough error analysis for *Spectrum* and compare it against previous local predictors, demonstrating tighter error bound at large time horizons. Notably, *Spectrum* admits an error bound that does not scale with the skip horizon. **3.** We propose a tractable and efficient method to fit the coefficients of the Chebyshev bases with negligible compute and memory overhead. **4.** We conduct extensive experiments on a suite of state-of-the-art image and video diffusion models. Results consistently verify that *Spectrum* yields remarkable speedups while maintaining much higher sample quality compared with previous feature caching approaches. Notably, *Spectrum* obtains up to  $4.79\times$  speedup on FLUX.1 and  $3.40$  to  $4.67\times$  speedup on Wan2.1-14B, all without notable quality degradation. These evidence favors our *Spectrum* as a solid step towards streamlined, real-time diffusion generation.

## 2. Related Work

Rich efforts have been taken to reduce the sampling latency of diffusion models, which we discuss as follows.

**Diffusion sampling acceleration via distillation.** This thread of works aims to distill multi-step teacher models into few-step students via additional training. Specifically, consistency models [45, 48] and subsequent efforts [14, 27] enforce consistency along the diffusion trajectory, while DMD [54, 55] and related works [38, 39] distill the student model by aligning with teacher score. Recent endeavors [6, 24, 35] adopt these techniques to flow matching models [20, 25] and have demonstrated success. While effective, these approaches require extra training and is prone to decreased diversity due to distillation, while our method is purely *training-free* and leaves the base denoiser intact.

**Diffusion sampling acceleration with ODE solvers.** Another family of work decreases the number of integration steps by leveraging more accurate ODE solvers of the probability flow ODE [47]. Pioneered by DDIM [44], various works, *e.g.*, DPMSolver [28, 29, 57], have introduced high-order solvers that simulate the reverse ODE with less error accumulation. Yet, when the number of sampling steps is extremely limited, they still deviate significantly from the original trajectory, leading to quality degradation. Our *Spectrum* is agnostic to the choice of solver and remains close to the reference trajectory by replacing unnecessary network evaluations with inexpensive forecasts.

**Diffusion acceleration by reusing cached features.** Most related to our present approach is the diffusion feature caching methods that avoid executing the denoiser at selected timesteps by using the cached features from historical activations. The simplest approach naively reuses the nearest cached latents [1, 40], which over-simplifies the feature correlation, leading to drops in sample quality. ToCa [61] and subsequent works [23, 58, 60] dynamically cache attention features. TeaCache [21] estimates time-dependent

input-output difference to actively decide when to cache, while recent works [7, 26, 30, 49] develop various dynamic caching strategies. Taylor-style forecasters improve upon this by discrete finite-difference expansions over a short temporal horizon [22]. However, their locality leads to large discretization error, making them less favorable in high speedup scenarios. Differently, *Spectrum* shifts from *local* time-domain approximations to *global* spectral forecasting, yielding better long-range behavior and more accurate simulation along the sampling trajectory.

**Other techniques.** A complementary stream reduces the cost per denoiser call through quantization [15, 18, 41], network pruning [5, 59], token reduction [2, 36, 56], or kernel-level optimizations [3]. Parallel sampling has also been explored that partitions and solves the trajectory with multiple cores [8, 42, 50]. These techniques are indeed orthogonal to our *Spectrum*, which can be potentially combined together to further improve the wall-clock performance.

## 3. Method

### 3.1. Feature Forecasting for Diffusion Acceleration

**Diffusion model and diffusion sampling.** Given a data point  $\mathbf{x} \in \mathcal{X} = \mathbb{R}^F$  sampled from the data distribution, diffusion models feature a forward process that progressively perturbs the input towards unit Gaussian noise  $\epsilon \sim \mathcal{N}(\mathbf{0}, \mathbf{I})$ . A neural network  $\epsilon_\theta : \mathcal{X} \times [0, 1] \mapsto \mathcal{X}$  is optimized to approach the score function  $\nabla_{\mathbf{x}} \log p_t(\mathbf{x})$  through, *e.g.*, denoising score matching [46, 47], where  $p_t$  is the marginal at time  $t$ . Critically, the sampling of diffusion models is grounded on the reverse process, typically parameterized by the probability-flow ODE [47]:

$$d\mathbf{x} = \left( f(t)\mathbf{x} - \frac{1}{2}g^2(t)\epsilon_\theta(\mathbf{x}, t) \right) dt, \quad (1)$$

where  $f(t)$  and  $g(t)$  are scalar functions specified by the noise schedule. Various types of ODE solvers [13, 28, 44] can be readily applied to simulate the ODE via, *e.g.*, discretizing uniformly over  $N$  timesteps  $\mathbb{T} = \{t_i\}_{i=1}^N$  with  $t_i = (i-1)\delta_t$ , where  $\delta_t = \frac{1}{N}$  is the interval between two adjacent timesteps. For instance, in the case of Euler solver, each step can be formulated as the following iteration:

$$\mathbf{x}_{t_{i+1}} = \text{Solve}(\mathbf{x}_{t_i}, \epsilon_\theta, t_i, t_{i+1}). \quad (2)$$

To obtain the clean data at  $t = 1$ , Eq. 2 will be iterated  $N$  times, leading to a total of  $N$  function calls to the denoiser  $\epsilon_\theta$ . Empirically, for the state-of-the-art diffusion models, the denoiser is usually parameterized by Diffusion Transformers [32] that comprise a sequential stack of dozens of attention blocks, making the entire sampling process compute-demanding and time-consuming.

**Feature caching and reusing.** To tackle the challenge, a line of works propose to cache the output features of the attention blocks at previous timesteps and reuse them to skip

the actual forward at future timesteps. Formally, we unify this class of algorithms as  $\mathcal{A} = (\mathbb{U}, \mathbb{V}, f)$  where  $\mathbb{U} \subseteq \mathbb{T}$  denotes the set of timesteps that requires the expensive forward pass of the denoiser  $\epsilon_\theta$ , and  $f$  is the forecaster whose output is employed as the surrogate of the network output for timesteps in  $\mathbb{V} = \mathbb{T} \setminus \mathbb{U}$ . Specifically, at certain timestep  $t_j \in \mathbb{V}$ , the forecaster  $f$  predicts the feature by using the cached features at the same block<sup>1</sup>:

$$\mathbf{h}_{t_j} = f(\mathbb{C}_{t_j}), \quad \text{s.t. } \mathbb{C}_{t_j} = \{(\mathbf{h}_{t_k}, t_k) : t_k < t_j, t_k \in \mathbb{U}\}, \quad (3)$$

where  $\mathbb{C}_{t_j}$  is the *feature cache* at the current timestep  $t_j$ , consisting of the features  $\mathbf{h}_{t_k} \in \mathbb{R}^F$  collected from actual passes of  $\epsilon_\theta$  at timesteps  $t_k \in \mathbb{U}$ . The theoretical speedup measured by the ratio of the number of network evaluations will be  $\eta = (\|\mathbb{U}\| + \|\mathbb{V}\|)/\|\mathbb{U}\| = \|\mathbb{T}\|/\|\mathbb{U}\|$ .

**Existing designs of  $\mathcal{A}$ .** Empirically, due to the strong temporal proximity of the latent features between adjacent timesteps, several designs of  $f$  have been found highly effective, including:

- Naive reusing [21, 40], which directly copies the cached feature at the nearest timestep  $t_k$  in  $\mathbb{C}_{t_j}$ , *i.e.*,  $f(\mathbb{C}_{t_j}) = \mathbf{h}_{t_k}$  where  $t_k = \max_t \{(\mathbf{h}, t) \in \mathbb{C}_{t_j}\}$ .
- TaylorSeer [22], which leverages a discrete Taylor expansion that predicts the feature based on  $P+1$  nearest cached timesteps:

$$\mathbf{h}_{t_j}^{\text{Taylor}} = \mathbf{h}_{t_k} + \sum_{p=1}^P \frac{\Delta^p \mathbf{h}_{t_k}}{p!} \left( \frac{j-k}{\eta} \right)^p, \quad (4)$$

where  $\Delta^p$  is the  $p$ -th order forward differential operator, which is defined as

$$\Delta^p \mathbf{h}_{t_k} = \sum_{i=0}^p (-1)^{p-i} \binom{p}{i} \mathbf{h}_{t_{k-i\eta}}, \quad p \leq \frac{k}{\eta}.$$

Notably, naive reusing can be viewed as the special case of TaylorSeer when the maximum order  $P = 0$ .

For the timesteps  $\mathbb{U}$  to perform an actual pass, the *fixed interval* strategy is commonly employed, *i.e.*,  $\mathbb{U} = \{(j-1)\eta\delta_t\}_{j=1}^{\lfloor N/\eta \rfloor}$  for speedup ratio  $\eta$  and unit timestep  $\delta_t$ .

### 3.2. From Local to Global: Bounding Forecasting Errors with Chebyshev Polynomials

**Pitfalls of the Taylor forecaster.** While demonstrated to be effective, from Eq. 4 it is evident that the prediction of the Taylor forecaster is grounded on discrete Taylor expansion using several most adjacent timesteps. Such a nature is prone to introducing a significantly growing approximation error when the forecasting step is large. Our observation is motivated by the following error analysis on the Taylor forecaster, as stated in the theorem below:

<sup>1</sup>We omit the block index  $l$  for conciseness.

**Theorem 3.1** (Worst-case error for local order- $P$  Taylor). *Fix an expansion point  $\tau_k \in [0, 1]$  and a target  $\tau_j = \tau_k + (j - k)\delta_t$ . Consider the smoothness class*

$$\mathcal{F}_{P+1}(L) = \{f \in C^{P+1}([0, 1]) : \|f^{(P+1)}\|_\infty \leq L\}, \quad L > 0.$$

*Let  $T_P[f](\tau_j)$  denote the ideal order- $P$  Taylor predictor of  $f(\tau_j)$  centered at  $\tau_k$  using the exact derivatives  $f^{(p)}(\tau_k)$ ,  $p \leq P$ . Then*

$$\sup_{f \in \mathcal{F}_{P+1}(L)} |f(\tau_j) - T_P[f](\tau_j)| = \frac{L}{(P+1)!} ((j-k)\delta_t)^{P+1}.$$

With the worst-case error, we locate the root cause that is detrimental to the forecasting accuracy of the Taylor method particularly when the speedup ratio  $\eta$  is high: the error will be dramatically amplified as the forecasting step size  $\tau_j - \tau_k$  increases, which leads to degraded sample quality for high speedups. This is due to the fact that the Taylor forecaster heavily relies on the features of the few adjacent timesteps as required by the local Taylor expansion, which is also highly ineffective in capturing the global, long-range spectral features produced along the entire sampling trajectory. Fig. 4 illustrates such an effect that the Taylor forecaster exaggerates the local sharp details while failing to capture the spectral features that are important to the overall semantics.

Realizing these clear limitations of the Taylor forecaster, we introduce *spectral feature forecasters*, which address the pitfalls above by switching to the spectral domain that models the sampling trajectory *globally*. At its core lies Chebyshev polynomials, a powerful tool that serves as a set of spectral bases for the temporal functions of our interest.

**Chebyshev polynomials.** Chebyshev polynomials of the first kind [31] are defined by the following recurrence,

$$T_m(\tau) = 2\tau T_{m-1}(\tau) - T_{m-2}(\tau), \quad (5)$$

with the base  $T_0(\tau) = 1$  and  $T_1(\tau) = \tau$  for  $\tau \in [-1, 1]$ . An important property of the Chebyshev polynomials is that they form a set of orthonormal basis for the function space, such that any function can be represented as a weighted sum of the Chebyshev polynomials:

**Theorem 3.2** (Universality of Chebyshev Polynomials). *Let  $f : [-1, 1] \rightarrow \mathbb{R}$  and let  $E_M(f) := \inf_{\deg(p) \leq M} \|f - p\|_\infty$ . If  $f$  extends analytically to the Bernstein ellipse  $E_\rho$  with parameter  $\rho > 1$  and  $\|f\|_{E_\rho} \leq B$ , then for the truncated Chebyshev series  $p_M$  of degree  $M$ ,*

$$\|f - p_M\|_\infty \leq \frac{2B}{\rho - 1} \rho^{-M}. \quad (6)$$

Theorem 3.2 states a critical property that lies in the heart of our spectral forecaster: Chebyshev polynomial approximates the target function uniformly regardless of the forecasting step size. Specifically, the approximation is bounded by the degree  $M$  as opposed to the step size, making our spectral forecaster much more robust to large step sizes enforced in high speedup scenarios.

### 3.3. Spectral Diffusion Feature Forecasting

With Chebyshev polynomials introduced, we are now ready to present the algorithm framework of our Spectral Feature Forecaster (*Spectrum*) for accelerating diffusion sampling. Specifically, we propose to view each channel of the feature vector<sup>2</sup> as a function that evolves through time  $t$ , i.e.,

$$\mathbf{h}_t = [h_1(t), \dots, h_F(t)] \in \mathbb{R}^F, \quad (7)$$

where  $h_i(t) : \mathbb{R} \mapsto \mathbb{R}$  is the function for the feature at channel  $i$ . For each  $h_i(t)$ , we leverage a set of Chebyshev polynomials up to degree  $M$  to approximate it, yielding

$$h_i(t) = \sum_{m=0}^M c_{m,i} T_m(\tau), \quad \text{s.t. } \tau = g(t), \quad (8)$$

where  $g(t) : [0, 1] \mapsto [-1, 1] = 2t - 1$  is the timestep projection that maps diffusion timestep to  $[-1, 1]$  to match the support of Chebyshev polynomials, and  $c_{m,i} \in \mathbb{R}$  is the coefficient for the  $m$ -th polynomial. Since we have no knowledge beforehand of the coefficients, we propose to fit them in an online manner during the sampling process.

**Online coefficient fitting.** For any timestep  $t_j$ , according to the protocol in Eq. 3 we have defined for  $\mathcal{A}$ , we have maintained the feature cache  $\mathbb{C}_{t_j}$  which consists of the features and timesteps collected from previous actual network evaluations. In order to perform the fitting, we first construct the basis row vector as

$$\phi(\tau_k) = [T_0(\tau_k), T_1(\tau_k), \dots, T_M(\tau_k)] \in \mathbb{R}^{M+1}, \quad (9)$$

which evaluates the Chebyshev polynomials at  $\tau_k = g(t_k)$  for all  $t_k$  recorded in  $\mathbb{C}_{t_j}$ . The design matrix  $\Phi_{t_j}$  is then instantiated as a stack of basis row vectors along time axis:

$$\Phi_{t_j} = [\phi(g(t_k))]_{(\mathbf{h}_{t_k}, t_k) \in \mathbb{C}_{t_j}} \in \mathbb{R}^{K \times (M+1)}, \quad (10)$$

where  $K = |\mathbb{C}_{t_j}|$  is the total number of currently cached timesteps. Similarly, the feature matrix is built by piling up the cached features over time:

$$\mathbf{H}_{t_j} = [\mathbf{h}_{t_k}]_{(\mathbf{h}_{t_k}, t_k) \in \mathbb{C}_{t_j}} \in \mathbb{R}^{K \times F}. \quad (11)$$

To obtain the coefficient matrix  $\mathbf{C}_{t_j} \in \mathbb{R}^{(M+1) \times F}$  that comprises the coefficients  $c_{m,i} = \mathbf{C}_{t_j}[m, i]$  used in Eq. 8, we solve the following ridge regression objective:

$$\mathbf{C}_{t_j} = \arg \min_{\mathbf{C}} \|\Phi_{t_j} \mathbf{C} - \mathbf{H}_{t_j}\|_F^2 + \lambda \|\mathbf{C}\|_F^2, \quad (12)$$

where  $\lambda \in \mathbb{R}$  is the regularization strength. It is worth noting that the regularization term is critical in terms of enhancing stability and relieving overfitting, as we will

<sup>2</sup>Here feature  $\mathbf{h}_t \in \mathbb{R}^F$  refers to the *fully flattened* network outputs.

---

**Algorithm 1** Adaptive Spectral Feature Forecaster

---

**Input:** Diffusion step  $N$ , timesteps  $\{t_j\}_{j=1}^N$ , denoiser  $\epsilon_\theta$ , initial latent  $\mathbf{x}_0$ , diffusion solver  $\text{Solve}(\cdot)$ .

```
1: for  $j = 1, \dots, N$  do
2:   if  $t_j \in \mathbb{U}$  then           ▷ If using actual forward pass
3:      $\mathbf{h}_{t_j}, \epsilon_{t_j} \leftarrow \epsilon_\theta(\mathbf{x}_{t_{j-1}}, t_{j-1})$   ▷ Actual forward pass
4:      $\mathbb{C}_{t_j} \leftarrow \mathbb{C}_{t_{j-1}} \cup \{(\mathbf{h}_{t_j}, t_j)\}$   ▷ Update feature cache
5:      $\mathbf{C}_{t_j} \leftarrow \text{Fit}(\mathbb{C}_{t_j})$   ▷ Eq. 10-13
6:   else                           ▷ If using our forecaster
7:      $\mathbf{C}_{t_j}, \mathbb{C}_{t_j} \leftarrow \mathbf{C}_{t_{j-1}}, \mathbb{C}_{t_{j-1}}$   ▷ Maintain the cache
8:      $\mathbf{h}_{t_j} \leftarrow \text{Forecast}(\mathbf{C}_{t_j}, t_j)$   ▷ Eq. 14
9:      $\epsilon_{t_j} \leftarrow \tilde{\epsilon}(\mathbf{h}_{t_j})$   ▷ Obtain the score
10:     $\mathbf{x}_{t_j} \leftarrow \text{Solve}(\mathbf{x}_{t_{j-1}}, \epsilon_{t_j}, t_{j-1}, t_j)$   ▷ Solver step
```

---

demonstrate in our experiment. The problem in Eq. 12 has the following close-form solution:

$$\mathbf{C}_{t_j} = \underbrace{(\Phi_{t_j}^\top \Phi_{t_j} + \lambda \mathbf{I})^{-1} \Phi_{t_j}^\top \mathbf{H}_{t_j}}_{\in \mathbb{R}^{(M+1) \times (M+1)}}, \quad (13)$$

which can be efficiently solved via Cholesky decomposition. Note that the matrix inversion term is of shape  $(M+1) \times (M+1)$ , which is negligible when the number of basis  $M$  remains small, compared with the feature dimension  $F$ , which is the major compute bound of the solve in Eq. 13. The basis fitting for  $\mathbf{C}_{t_j}$  can be naturally conducted in an online manner. Whenever a new latent feature is produced from  $\epsilon_\theta$ , we update  $\mathbf{C}_{t_j}$  by solving Eq. 13 and cache the updated coefficients, which will be leveraged to forecast the features at future timesteps.

**Feature forecasting with fitted coefficients.** For the timesteps  $t_j \in \mathbb{V}$ , the algorithm skips the network pass of  $\epsilon_\theta$  and inherits the cached coefficients  $\mathbf{C}_{t_j} = \mathbf{C}_{t_{j-1}}$  to forecast the feature value at current timestep, following Eq. 8:

$$\mathbf{h}_{t_j} = \phi(g(t_j))\mathbf{C}_{t_j}. \quad (14)$$

The predicted  $\mathbf{h}_{t_j}$  is then directly ensembled throughout the network to produce the estimated score  $\epsilon_{t_j}$  for the current step without any expensive full pass over the network.

**Overall procedure.** As depicted in Alg. 1, our *Spectrum* operates in an online fitting-then-forecasting manner. Specifically, for each sampling step  $j$  looping through 1 to  $N$ , if  $t_j \in \mathbb{U}$ , we perform one actual network pass through the denoiser  $\epsilon_\theta$  to obtain the latent features  $\mathbf{h}_{t_j}$  as well as the output score  $\epsilon_{t_j}$ . The features  $\mathbf{h}_{t_j}$  will be cached and the Chebyshev coefficients  $\mathbf{C}_{t_j}$  will be updated correspondingly by solving Eq. 13. Otherwise, for  $t_j \in \mathbb{V}$ , we spare one network evaluation by directly predicting the features via Eq. 14 using the previously computed coefficients.

### 3.4. Analysis and Extensions

In this subsection, we provide more detailed discussions on *Spectrum*, including time and memory complexity anal-

ysis. We further propose several empirical extensions of *Spectrum* that further enhances its practical performance.

**Error analysis.** Theorem 3.3 below shows an error bound of *Spectrum*, which is an extension of Theorem 3.2. Notably, it does not depend on the step size  $\tau_j - \tau_k$  as in the Taylor forecaster, which is highly beneficial.

**Theorem 3.3** (Error Bound of *Spectrum*). *Using the notation in Sec. 3, fix a channel  $i$  and write  $f(\tau) = h_i(t)$  with  $\tau = g(t) \in [-1, 1]$ . Assume  $f$  extends analytically to the Bernstein ellipse  $E_\rho$  with  $\rho > 1$  and  $\|f\|_{E_\rho} \leq B$ . Let  $p_M$  be the degree- $M$  Chebyshev truncation of  $f$  and  $\varepsilon_M := \|f - p_M\|_\infty \leq \frac{2B}{\rho-1} \rho^{-M}$  as in Theorem 3.2. For a forecast step  $t_j$  with cache  $\mathbb{C}_{t_j}$ , let  $\hat{h}_i(t_j)$  be the *Spectrum* predictor at time  $t_j$  obtained from Eq. 14 using the fitted coefficients  $\mathbf{C}_{t_j}$  from Eq. 13. Then for any forecast time  $t_j$  with  $\tau_j = g(t_j)$ ,*

$$\begin{aligned} & |h_i(t_j) - \hat{h}_i(t_j)| \\ & \leq \varepsilon_M \left( 1 + \frac{(M+1)K}{\sigma_{\min}(\Phi_{t_j})^2 + \lambda} \right) + \frac{\lambda \sqrt{M+1}}{\sigma_{\min}(\Phi_{t_j})^2 + \lambda} \cdot \frac{2B}{\sqrt{1-\rho^{-2}}}, \end{aligned}$$

where  $\sigma_{\min}(\Phi_{t_j})$  is the smallest singular value of  $\Phi_{t_j}$ .

**Complexity.** For time complexity, the fitting in Eq. 13 is of  $\mathcal{O}(K(M+1)^2 + K(M+1)F + (M+1)^3 + (M+1)^2F)$ , where  $K$  is the number of cached timesteps,  $M$  is the degree of Chebyshev basis, and  $F$  is the latent feature dimension. Empirically, we have  $M \ll K \ll F$ , making  $\mathcal{O}(K(M+1)F)$  the dominant term. Compared with the Taylor forecaster, which is of complexity  $\mathcal{O}(PF)$  where  $P$  is the Taylor expansion order, *Spectrum* only incurs marginal compute overhead, which is only of magnitude  $K(M+1)/P$ . The forecast operation in Eq. 14 is merely  $\mathcal{O}((M+1)F)$ . Practically, both  $K$  and  $M$  are particularly small, making the overhead negligible, especially compared with the extremely computationally intensive operations in the actual denoiser forward passes. Regarding the memory, we only need to additionally preserve the coefficients matrix  $\mathbf{C}$  besides the features in the cache  $\mathbb{C}$ , which leads to a total of  $\mathcal{O}((M+1)F + KF)$  memory occupation.

**Caching the final block.** The original Taylor forecaster [22] maintains a cache for *each modules* in attention blocks, which introduces  $L$  times more memory and compute overhead where  $L$  is the number of blocks. In practice, we find the layer-wise design redundant, and we instead only instantiate *Spectrum* for the output of the final attention block. Through extensive experiments, we verify that this strategy consistently yields on par or even better sample quality compared with layer-wise caching, while significantly reducing compute and memory overhead.

**Adaptive scheduling.** Since the diffusion sampling procedure in Alg. 1 is indeed performed iteratively from  $t = 0$  to 1, the approximation errors of the forecaster induced in early diffusion steps will accumulate in the later steps, significantly amplifying the final error. To this end, we also

Table 1. Benchmark results of **text-to-image generation** task on DrawBench with Flux and Stable Diffusion 3.5-Large. We use 50 steps as the reference ( $\dagger$ ). Our *Spectrum* achieves higher speedup while maintaining better sample quality across two speedup scenarios consistently.

	FLUX.1 [17]						Stable Diffusion 3.5-Large [4]							
	Acceleration		Quality			Image Reward $\uparrow$	CLIP $\uparrow$	Acceleration		Quality			Image Reward $\uparrow$	CLIP $\uparrow$
	Latency(s) $\downarrow$	Speedup $\uparrow$	PSNR $\uparrow$	SSIM $\uparrow$	LPIPS $\downarrow$			Latency(s) $\downarrow$	Speedup $\uparrow$	PSNR $\uparrow$	SSIM $\uparrow$	LPIPS $\downarrow$		
50 steps $\dagger$	26.03	1.00	-	-	-	1.00	27.49	25.05	1.00	-	-	-	1.05	28.66
25 steps	13.23	1.97	18.11	0.752	0.322	1.01	27.58	12.67	1.98	12.41	0.593	0.464	1.02	28.78
15 steps	8.04	3.24	15.77	0.673	0.432	1.00	27.56	7.71	3.25	10.51	0.453	0.595	0.85	28.75
FORA ( $\mathcal{N} = 4$ ) [40]	8.40	3.19	15.15	0.651	0.454	0.97	27.55	8.63	2.90	9.54	0.437	0.606	0.27	27.03
ToCa ( $\mathcal{N} = 4, \mathcal{R} = 0.9$ ) [61]	16.93	1.58	17.18	0.724	0.362	<b>1.03</b>	27.63	17.27	1.45	10.55	0.483	0.557	0.51	27.19
TeaCache ( $\delta = 0.4$ ) [21]	10.66	2.44	18.70	0.762	0.311	<b>1.03</b>	<b>27.68</b>	10.75	2.33	11.89	0.527	0.512	0.78	27.46
TaylorSeer ( $\mathcal{N} = 4, \mathcal{O} = 1$ ) [22]	8.55	3.13	22.31	0.841	<b>0.215</b>	0.99	27.60	8.75	2.86	13.13	0.605	0.428	0.82	27.91
TaylorSeer ( $\mathcal{N} = 4, \mathcal{O} = 2$ ) [22]	8.59	3.03	20.76	0.812	0.247	1.02	27.61	8.70	2.88	11.12	0.513	0.529	0.44	27.24
<i>Spectrum</i> ( $\alpha = 0.75$ )	<b>7.73</b>	<b>3.47</b>	<b>24.32</b>	<b>0.854</b>	0.217	0.99	27.65	<b>7.82</b>	<b>3.21</b>	<b>17.83</b>	<b>0.743</b>	<b>0.305</b>	<b>0.97</b>	<b>28.61</b>
FORA ( $\mathcal{N} = 6$ ) [40]	6.49	4.13	14.33	0.613	0.505	0.85	27.30	6.73	3.72	9.05	0.389	0.687	0.02	26.19
ToCa ( $\mathcal{N} = 6, \mathcal{R} = 0.9$ ) [61]	13.38	1.95	16.49	0.666	0.439	0.99	27.61	13.99	1.79	9.53	0.446	0.611	0.17	26.33
TeaCache ( $\delta = 0.8$ ) [21]	6.75	3.85	16.71	0.695	0.406	<b>1.00</b>	27.63	7.17	3.49	10.04	0.472	0.589	0.39	27.08
TaylorSeer ( $\mathcal{N} = 6, \mathcal{O} = 1$ ) [22]	6.48	4.14	20.24	0.785	0.294	<b>1.00</b>	27.60	6.78	3.69	11.18	0.505	0.535	0.32	27.27
TaylorSeer ( $\mathcal{N} = 6, \mathcal{O} = 2$ ) [22]	6.52	3.99	17.41	0.708	0.389	0.99	27.39	6.76	3.71	9.36	0.429	0.636	0.10	25.90
<i>Spectrum</i> ( $\alpha = 3.0$ )	<b>5.60</b>	<b>4.79</b>	<b>22.21</b>	<b>0.788</b>	<b>0.261</b>	<b>1.00</b>	<b>27.64</b>	<b>5.81</b>	<b>4.32</b>	<b>15.68</b>	<b>0.620</b>	<b>0.430</b>	<b>0.82</b>	<b>28.00</b>

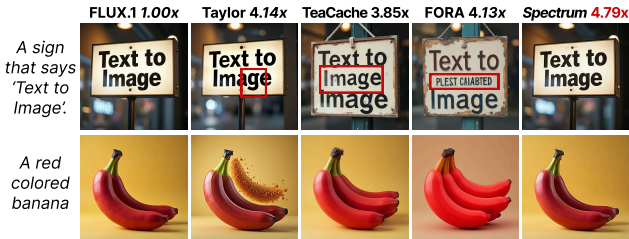


Figure 2. **Qualitative comparison on text-to-image generation** using FLUX.1. *Spectrum* aligns consistently with the 50-step reference while accelerating it by a factor of 4.79 $\times$ . Other baselines show noticeable degradation in color and prompt consistency.

introduce an adaptive timestep scheduler that encourages more actual network passes at the early sampling stage and gradually increases the usage of the forecaster at later diffusion steps. Specifically, for a total of  $N$  diffusion steps, we select  $\mathbb{U} = \{\tau_j : j = \lfloor \alpha \frac{r(r+1)}{2} \rfloor, r \in \mathbb{N}^+, 1 \leq j \leq N\}$  where  $\alpha \geq 0$  is the slope of the time interval between adjacent timesteps in  $\mathbb{U}$ . More explanations are in the Appendix.

## 4. Experiments

In this section, we benchmark our spectral feature forecaster against existing cache-then-predict approaches on both text-to-image generation (Sec. 4.1) and text-to-video generation (Sec. 4.2). Furthermore, we ablate our key designs and verify the efficacy of each component in Sec. 4.3.

### 4.1. Accelerating Text-to-Image Diffusion Models

**Experiment setup.** For text-to-image generation, we benchmark on two state-of-the-art image diffusion models, FLUX.1-dev [17] and Stable Diffusion 3.5-Large [4]. We by default adopt 50 sampling steps as the reference, following established configurations. Experiments are performed on NVIDIA A100 GPUs for this task. We employ DrawBench [37] as the prompt suite which contains 200 prompts, and we set the image resolution to 1024 $\times$ 1024 for both

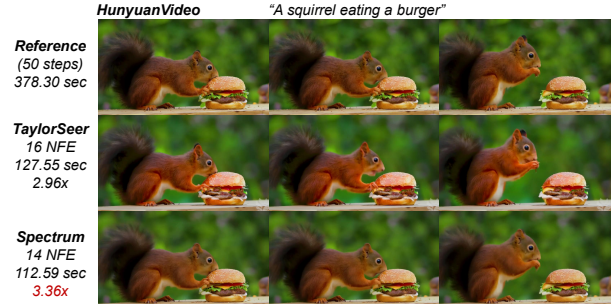


Figure 3. **Qualitative comparisons on HunyuanVideo.** *Spectrum* achieves higher sample fidelity while delivering more speedup.

models. We by default set  $\lambda = 0.1$  and  $M = 4$  for *Spectrum* with detailed ablations presented in Sec. 4.3.

**Baselines.** We compare *Spectrum* against the following baselines:  $\kappa$  steps, where we naively reduce the sampling step to  $\kappa \leq 50$ ; FORA [40] and ToCa [61], which rely on direct cache reuse; TeaCache, which employs a dynamic caching scheduling; and TaylorSeer [22], which predicts future cache values using Taylor expansion. We comprehensively benchmark the methods in two scenarios with different speedups controlled by their hyperparameters  $\mathcal{N}$  and  $\alpha$ . In particular,  $\mathcal{N} = 4$  and  $\mathcal{N} = 6$  correspond to 16 and 12 network evaluations, while  $\alpha = 0.75$  and  $\alpha = 3.0$  imply 14 and 10 network evaluations, respectively.

**Metrics.** We report the sampling latency (seconds per image) and the empirical speedup compared with the original 50-step sampler. For image quality, we first evaluate PSNR, SSIM, LPIPS between the generated images for each approach and the reference images generated by the 50-step sampler. We also include the ImageReward [52] and CLIP Score [9] of the generated images.

**Qualitative comparison.** We provide visualization of the generated videos on Hunyuan and Wan in Fig. 3 and 4, respectively (more in appendix). While TaylorSeer clearly exhibits unexpected artifacts on both the character and back-

Table 2. Benchmark results of **text-to-video generation** task on VBench with Wan2.1-14B and HunyuanVideo. We use 50 steps as the reference ( $\dagger$ ). Our *Spectrum* achieves higher speedup while maintaining better sample quality across two speedup scenarios consistently.

	Wan2.1-14B [51]						HunyuanVideo [16]					
	Acceleration		Quality			VBench Quality $\uparrow$	Acceleration		Quality			VBench Quality $\uparrow$
	Latency(s) $\downarrow$	Speedup $\uparrow$	PSNR $\uparrow$	SSIM $\uparrow$	LPIPS $\downarrow$		Latency(s) $\downarrow$	Speedup $\uparrow$	PSNR $\uparrow$	SSIM $\uparrow$	LPIPS $\downarrow$	
50 steps $\dagger$	486.12	1.00	-	-	-	83.15	378.30	1.00	-	-	-	84.61
25 steps	246.30	1.97	14.94	0.459	0.481	81.74	193.19	1.96	19.64	0.673	0.376	84.78
15 steps	150.50	3.23	13.92	0.397	0.546	80.77	119.58	3.16	17.40	0.620	0.459	83.21
FORA ( $\mathcal{N} = 4$ ) [40]	155.80	3.12	14.47	0.426	0.532	80.53	122.42	3.09	18.24	0.663	0.427	83.34
ToCa ( $\mathcal{N} = 4, \mathcal{R} = 0.9$ ) [61]	313.62	1.55	16.88	0.537	0.410	82.18	247.25	1.53	21.26	0.732	0.357	83.79
TeaCache ( $\delta = 0.2$ ) [21]	164.78	2.95	19.13	0.628	0.347	82.59	130.44	2.90	23.88	0.783	0.270	84.08
TaylorSeer ( $\mathcal{N} = 4, \mathcal{O} = 1$ ) [22]	161.50	3.01	19.46	0.660	0.299	82.74	127.55	2.96	24.73	0.805	0.243	84.03
<i>Spectrum</i> ( $\alpha = 0.75$ )	<b>143.03</b>	<b>3.40</b>	<b>22.78</b>	<b>0.749</b>	<b>0.222</b>	<b>82.80</b>	<b>112.59</b>	<b>3.36</b>	<b>27.77</b>	<b>0.842</b>	<b>0.209</b>	<b>84.11</b>
FORA ( $\mathcal{N} = 6$ ) [40]	120.92	4.02	13.02	0.353	0.598	80.82	95.77	3.95	17.29	0.594	0.475	83.35
ToCa ( $\mathcal{N} = 6, \mathcal{R} = 0.9$ ) [61]	250.57	1.94	15.10	0.488	0.453	81.14	199.10	1.90	19.48	0.656	0.438	83.62
TeaCache ( $\delta = 0.25$ ) [21]	127.59	3.81	16.53	0.557	0.390	81.85	102.52	3.69	21.42	0.725	0.334	83.68
TaylorSeer ( $\mathcal{N} = 6, \mathcal{O} = 1$ ) [22]	123.49	3.94	17.24	0.585	0.367	81.38	97.83	3.86	22.27	0.740	0.303	83.40
<i>Spectrum</i> ( $\alpha = 3.0$ )	<b>104.18</b>	<b>4.67</b>	<b>21.24</b>	<b>0.694</b>	<b>0.265</b>	<b>82.21</b>	<b>82.90</b>	<b>4.56</b>	<b>25.39</b>	<b>0.779</b>	<b>0.273</b>	<b>83.89</b>



Figure 4. **Qualitative comparison on text-to-video generation** using Wan2.1-14B. *Spectrum* aligns consistently with the high-quality 50-step reference using only 14 network evaluations, while TaylorSeer is slower and exhibits noticeable artifacts on character and background.

ground, *Spectrum* consistently remains high-quality and aligns accurately with the reference 50-step samples.

**Results.** The quantitative results are presented in Table 1. Notably, *Spectrum* consistently achieves higher speedup while maintaining much better sample quality compared with all baselines, demonstrating the efficacy of our spectral feature forecaster. Furthermore, TaylorSeer encounters severe quality degradation in the higher speedup scenario ( $\alpha = 3.0$  or  $\mathcal{N} = 6$ ) with remarkable drops in the quality metrics (e.g., 0.82 to 0.32 on ImageReward with SD3.5) due to the enlarged error in the approximation. Naively increasing the order of TaylorSeer does not address the problem, which aligns with our analysis. In contrast, our *Spectrum* remains robust across all speedups, achieving much higher quality while using fewer network evaluations, thanks to the spectral forecasting approach with bounded error and better long-horizon behavior. Remarkably, *Spectrum* ( $\alpha = 3.0$ ) achieves nearly the same PSNR with TaylorSeer ( $\mathcal{N} = 4$ ), while only using 10 network evaluations as opposed to 16.

## 4.2. Accelerating Text-to-Video Diffusion Models

**Experiment setup.** We further evaluate *Spectrum* on two advanced text-to-video diffusion models, Wan2.1-14B [51]

and HunyuanVideo [16]. We adopt VBench [12] as the benchmark suite and directly leverage their prompt set and evaluation protocol. The inference for all approaches is conducted on NVIDIA H800 GPUs. Besides PSNR, SSIM, and LPIPS, we also report the VBench Quality Score (%) as a quantitative measurement of video quality.

**Results.** As depicted in Table 2, *Spectrum* exhibits exceptional effectiveness on text-to-video generation, achieving up to  $4.67\times$  wallclock speedup with negligible effect on quality scores. While the quality drops even more significantly for the baselines, with TaylorSeer merely getting a PSNR of 17.24 on Wan2.1-14B, our *Spectrum* keeps producing high-fidelity video samples, reaching 21.24 PSNR with only 10 network passes. The superior quality obtained with extremely limited number of network evaluations again endorses our core design of modeling the latent features with spectral basis.

## 4.3. Ablation Studies

**The effect of regularization weight  $\lambda$ .** As depicted in Eq. 13, the factor  $\lambda$  serves as the regularization strength in the ridge regression problem. Here we investigate the empirical effect of  $\lambda$  on FLUX.1 under different speedups by

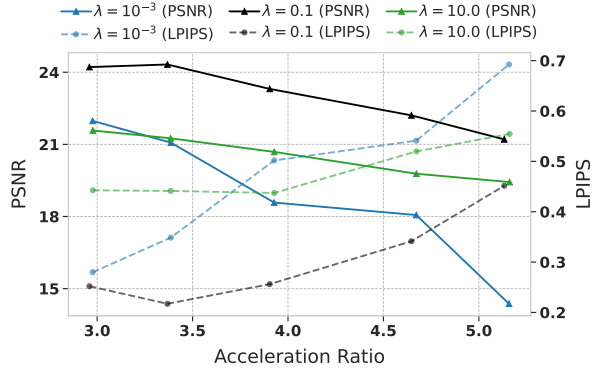


Figure 5. Ablation study on the regularization weight  $\lambda$ .

Table 3. Ablation study of adaptive scheduling on SD3.5 and Wan.

Stable Diffusion 3.5-Large [4]					
	Adaptive	PSNR $\uparrow$	SSIM $\uparrow$	LPIPS $\downarrow$	Image Reward $\uparrow$
Taylor ( $\mathcal{N} = 8$ )	×	10.40	0.460	0.594	-0.22
Taylor ( $\alpha = 3.0$ )	✓	13.25	0.585	0.454	0.65
Spectrum ( $\mathcal{N} = 8$ )	×	11.34	0.501	0.552	0.23
Spectrum ( $\alpha = 3.0$ )	✓	<b>15.68</b>	<b>0.620</b>	<b>0.430</b>	<b>0.82</b>

Wan2.1-14B [51]					
	Adaptive	PSNR $\uparrow$	SSIM $\uparrow$	LPIPS $\downarrow$	VBench Score $\uparrow$
Taylor ( $\mathcal{N} = 8$ )	×	17.24	0.584	0.367	81.38
Taylor ( $\alpha = 3.0$ )	✓	19.85	0.674	0.283	81.67
Spectrum ( $\mathcal{N} = 8$ )	×	20.65	0.687	0.275	<b>82.32</b>
Spectrum ( $\alpha = 3.0$ )	✓	<b>21.24</b>	<b>0.694</b>	<b>0.265</b>	82.21

sweeping over  $\alpha$ , with results in Fig. 5. It is observed that both  $\lambda = 10^{-3}$  and  $\lambda = 10$  lead to detriment of image quality at each acceleration ratio, since a large  $\lambda$  leads to underfitting of the features and hence larger forecasting error, while a small  $\lambda$  adds insufficient diagonal regularization and incurs numerical instability when solving Eq. 13.

**The effect of adaptive scheduling.** We further study the efficacy of our proposed adaptive scheduling strategy, with results displayed in Table 3. Notably, using the same number of network evaluations, our adaptive scheduling ( $\alpha = 3.0$ ) yields enhanced sample quality compared with fixed step-size scheduling ( $\mathcal{N} = 8$ ) as evidenced by higher PSNR, SSIM, and Image Reward. The improvement remains consistent across both Taylor and our spectral forecaster, further validating our proposal. It is worth highlighting that *Spectrum* significantly promotes the sample quality over TaylorSeer regardless of the scheduling. For instance, *Spectrum* enhances PSNR from 17.24 to 20.65 on Wan2.1 even under the fixed scheduling ( $\mathcal{N} = 8$ ), which, again, verifies the efficacy and robustness of our spectral forecaster.

**Ablation on the degree of Chebyshev polynomials  $M$ .** Per our analysis, the degree of Chebyshev polynomials,  $M$ , is a key factor: A small  $M$  will lead to imprecise modeling of the function  $h_i(t)$  and thus incurs more forecasting error, while a large  $M$  may bring unnecessary computation and memory overhead. The empirical observations on FLUX.1 in Fig. 6 well align with our analysis. The sample quality is promoted as  $M$  increases from 2 to 4, while further scaling up  $M$  to 6 brings marginal improvement. We therefore

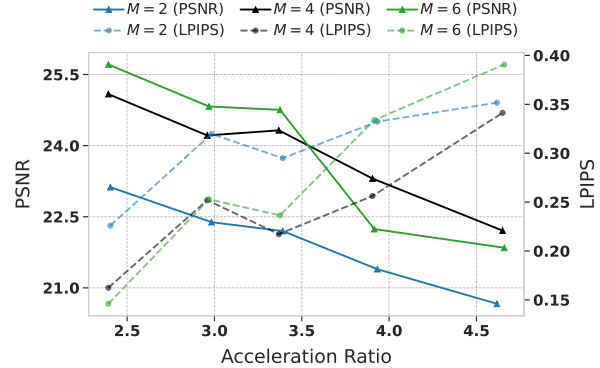


Figure 6. Ablation on the degree of Chebyshev polynomials  $M$ .

Table 4. Ablation study of the last-block-only caching strategy on FLUX.1 with  $\mathcal{N} = 8$  for both Taylor and *Spectrum*.

	Last only	Latency(s) $\downarrow$	PSNR $\uparrow$	SSIM $\uparrow$	LPIPS $\downarrow$	Image Reward $\uparrow$
Taylor	×	7.36	17.93	0.718	0.375	0.99
Taylor	✓	5.45	18.61	0.738	0.356	0.99
Spectrum	×	15.44	19.34	0.725	0.362	1.02
Spectrum	✓	5.59	19.66	0.741	0.341	1.03

Table 5. RMSE between predicted latents and oracle on Wan2.1.

Diffusion step	10	20	30	40	50
Taylor ( $\mathcal{N} = 8$ )	0.0121	0.0303	0.0629	0.1226	0.2510
Spectrum ( $\alpha = 3.0$ )	0.0040	0.0164	0.0358	0.0742	0.1674

adopt the choice of  $M = 4$  which is sufficiently effective for modeling the per-channel scalar temporal function  $h_i(t)$ .

**The effect of direct last-block forecasting.** Empirically, we propose to only cache and forecast the output features from the last attention block. We validate such proposal in Table 4 by controlling  $\mathcal{N} = 8$ . Specifically, compared with the original TaylorSeer, which performs caching and forecasting per module, operating only for the last block surprisingly yields even better performance while being much faster also more memory-efficient. We speculate that per-module forecasting incurs more frequent error accumulation when aggregating predicted features while the last-block-only modeling removes such redundancy.

**Feature-level analysis.** We evaluate the RMSE between the latents produced by the 50-step oracle and the forecasters at different diffusion steps in Table 5, which clearly shows that our spectral predictor produces diffusion features that are much closer to the oracle. More results are in Appendix.

## 5. Conclusion

We introduce *Spectrum*, a training-free diffusion sampling acceleration technique that caches and forecasts latent features in the denoiser. Our core idea is to approximate latent features with Chebyshev polynomials, leading to a spectral forecaster with controlled error bound. Extensive experiments on image and video diffusion models demonstrate that *Spectrum* can preserve high sample quality with much fewer network evaluations. *Spectrum* takes a solid step toward high-throughput, real-time diffusion generation.

**Acknowledgments.** We thank the anonymous reviewers for their feedback on improving the manuscript. This work was supported by ARO (W911NF-21-1-0125), ONR (N00014-23-1-2159), and the CZ Biohub.

## References

- [1] Pengtao Chen, Mingzhu Shen, Peng Ye, Jianjian Cao, Chongjun Tu, Christos-Savvas Bouganis, Yiren Zhao, and Tao Chen.  $\delta$ -dit: A training-free acceleration method tailored for diffusion transformers. *arXiv preprint arXiv:2406.01125*, 2024. 2
- [2] Xinle Cheng, Zhuoming Chen, and Zhihao Jia. Cat pruning: Cluster-aware token pruning for text-to-image diffusion models, 2025. 3
- [3] Tri Dao, Daniel Y. Fu, Stefano Ermon, Atri Rudra, and Christopher R'e. Flashattention: Fast and memory-efficient exact attention with io-awareness. *ArXiv*, abs/2205.14135, 2022. 3
- [4] Patrick Esser, Sumith Kulal, Andreas Blattmann, Rahim Entezari, Jonas Müller, Harry Saini, Yam Levi, Dominik Lorenz, Axel Sauer, Frederic Boesel, et al. Scaling rectified flow transformers for high-resolution image synthesis. In *Forty-first international conference on machine learning*, 2024. 1, 6, 8
- [5] Gongfan Fang, Xinyin Ma, and Xinchao Wang. Structural pruning for diffusion models. *arXiv preprint arXiv:2305.10924*, 2023. 3
- [6] Zhengyang Geng, Mingyang Deng, Xingjian Bai, J Zico Kolter, and Kaiming He. Mean flows for one-step generative modeling. *arXiv preprint arXiv:2505.13447*, 2025. 2
- [7] Xiaoliu Guan, Lielin Jiang, Hanqi Chen, Xu Zhang, Jiaying Yan, Guanzhong Wang, Yi Liu, Zetao Zhang, and Yu Wu. Forecasting when to forecast: Accelerating diffusion models with confidence-gated taylor. *Knowledge-Based Systems*, page 114635, 2025. 3
- [8] Jiaqi Han, Haotian Ye, Puheng Li, Minkai Xu, James Zou, and Stefano Ermon. Chords: Diffusion sampling accelerator with multi-core hierarchical ode solvers. In *Proceedings of the IEEE/CVF International Conference on Computer Vision*, pages 19386–19395, 2025. 3
- [9] Jack Hessel, Ari Holtzman, Maxwell Forbes, Ronan Le Bras, and Yejin Choi. CLIPScore: a reference-free evaluation metric for image captioning. In *EMNLP*, 2021. 6
- [10] Jonathan Ho, Ajay Jain, and Pieter Abbeel. Denoising diffusion probabilistic models. *Advances in neural information processing systems*, 33:6840–6851, 2020. 1
- [11] Ziqi Huang, Yanan He, Jiashuo Yu, Fan Zhang, Chenyang Si, Yuming Jiang, Yuanhan Zhang, Tianxing Wu, Qingyang Jin, Nattapol Chanpaisit, Yaohui Wang, Xinyuan Chen, Limin Wang, Dahua Lin, Yu Qiao, and Ziwei Liu. VBench: Comprehensive Benchmark Suite for Video Generative Models, 2023. arXiv:2311.17982 [cs]. 14
- [12] Ziqi Huang, Yanan He, Jiashuo Yu, Fan Zhang, Chenyang Si, Yuming Jiang, Yuanhan Zhang, Tianxing Wu, Qingyang Jin, Nattapol Chanpaisit, Yaohui Wang, Xinyuan Chen, Limin Wang, Dahua Lin, Yu Qiao, and Ziwei Liu. VBench: Comprehensive benchmark suite for video generative models. In *Proceedings of the IEEE/CVF Conference on Computer Vision and Pattern Recognition*, 2024. 7
- [13] Tero Karras, Miika Aittala, Timo Aila, and Samuli Laine. Elucidating the design space of diffusion-based generative models. *Advances in Neural Information Processing Systems*, 35:26565–26577, 2022. 3
- [14] Dongjun Kim, Chieh-Hsin Lai, Wei-Hsiang Liao, Naoki Murata, Yuhta Takida, Toshimitsu Uesaka, Yutong He, Yuki Mitsufuji, and Stefano Ermon. Consistency trajectory models: Learning probability flow ode trajectory of diffusion. *arXiv preprint arXiv:2310.02279*, 2023. 2
- [15] Sungbin Kim, Hyunwuk Lee, Wonho Cho, Mincheol Park, and Won Woo Ro. Ditto: Accelerating diffusion model via temporal value similarity. In *Proceedings of the 2025 IEEE International Symposium on High-Performance Computer Architecture (HPCA)*. IEEE, 2025. 3
- [16] Weijie Kong, Qi Tian, Zijian Zhang, Rox Min, Zuozhuo Dai, Jin Zhou, Jiangfeng Xiong, Xin Li, Bo Wu, Jianwei Zhang, et al. Hunyuanvideo: A systematic framework for large video generative models. *arXiv preprint arXiv:2412.03603*, 2024. 7
- [17] Black Forest Labs. Flux. <https://github.com/black-forest-labs/flux>, 2024. 6, 16
- [18] Xiuyu Li, Yijiang Liu, Long Lian, Huanrui Yang, Zhen Dong, Daniel Kang, Shanghang Zhang, and Kurt Keutzer. Q-diffusion: Quantizing diffusion models. In *Proceedings of the IEEE/CVF International Conference on Computer Vision*, pages 17535–17545, 2023. 3
- [19] Tsung-Yi Lin, Michael Maire, Serge Belongie, James Hays, Pietro Perona, Deva Ramanan, Piotr Dollár, and C Lawrence Zitnick. Microsoft coco: Common objects in context. In *Computer Vision—ECCV 2014: 13th European Conference, Zurich, Switzerland, September 6-12, 2014, Proceedings, Part V 13*, pages 740–755. Springer, 2014. 16
- [20] Yaron Lipman, Ricky T. Q. Chen, Heli Ben-Hamu, Maximilian Nickel, and Matthew Le. Flow matching for generative modeling. In *The Eleventh International Conference on Learning Representations*, 2023. 2
- [21] Feng Liu, Shiwei Zhang, Xiaofeng Wang, Yujie Wei, Haonan Qiu, Yuzhong Zhao, Yingya Zhang, Qixiang Ye, and Fang Wan. Timestep embedding tells: It's time to cache for video diffusion model, 2024. 2, 3, 6, 7, 14, 16
- [22] Jiacheng Liu, Chang Zou, Yuanhuiyi Lyu, Junjie Chen, and Linfeng Zhang. From reusing to forecasting: Accelerating diffusion models with taylorseers. In *Proceedings of the IEEE/CVF International Conference on Computer Vision (ICCV)*, pages 15853–15863, 2025. 2, 3, 5, 6, 7, 14, 16
- [23] Jiacheng Liu, Chang Zou, Yuanhuiyi Lyu, Kaixin Li, Shaobo Wang, and Linfeng Zhang. Specra: Accelerating diffusion transformers with speculative feature caching. In *Proceedings of the 33rd ACM International Conference on Multimedia (MM '25)*, page to appear, Dublin, Ireland, 2025. ACM. 2
- [24] Xingchao Liu, Chengyue Gong, and qiang liu. Flow straight and fast: Learning to generate and transfer data with rectified flow. In *The Eleventh International Conference on Learning Representations*, 2023. 2

- [25] Xingchao Liu, Chengyue Gong, et al. Flow straight and fast: Learning to generate and transfer data with rectified flow. In *The Eleventh International Conference on Learning Representations*, 2023. 2
- [26] Ziming Liu, Yifan Yang, Chengruidong Zhang, Yiqi Zhang, Lili Qiu, Yang You, and Yuqing Yang. Region-adaptive sampling for diffusion transformers, 2025. 2, 3, 14
- [27] Cheng Lu and Yang Song. Simplifying, stabilizing and scaling continuous-time consistency models. In *The Thirteenth International Conference on Learning Representations*, 2025. 2
- [28] Cheng Lu, Yuhao Zhou, Fan Bao, Jianfei Chen, Chongxuan Li, and Jun Zhu. Dpm-solver: A fast ode solver for diffusion probabilistic model sampling in around 10 steps. *Advances in Neural Information Processing Systems*, 35:5775–5787, 2022. 2, 3
- [29] Cheng Lu, Yuhao Zhou, Fan Bao, Jianfei Chen, Chongxuan Li, and Jun Zhu. Dpm-solver++: Fast solver for guided sampling of diffusion probabilistic models. *arXiv preprint arXiv:2211.01095*, 2022. 2
- [30] Zhengyao Lv, Chenyang Si, Junhao Song, Zhenyu Yang, Yu Qiao, Ziwei Liu, and Kwan-Yee K. Wong. Faster-Cache: Training-Free Video Diffusion Model Acceleration with High Quality, 2025. 2, 3, 14
- [31] John C Mason and David C Handscomb. *Chebyshev polynomials*. Chapman and Hall/CRC, 2002. 2, 4
- [32] William Peebles and Saining Xie. Scalable diffusion models with transformers, 2023. 2, 3
- [33] Theodore J Rivlin et al. The chebyshev polynomials, pure and applied mathematics, 1974. 2
- [34] Robin Rombach, Andreas Blattmann, Dominik Lorenz, Patrick Esser, and Björn Ommer. High-resolution image synthesis with latent diffusion models. In *Proceedings of the IEEE/CVF conference on computer vision and pattern recognition*, pages 10684–10695, 2022. 1
- [35] Amirmojtaba Sabour, Sanja Fidler, and Karsten Kreis. Align your flow: Scaling continuous-time flow map distillation. *arXiv preprint arXiv:2506.14603*, 2025. 2
- [36] Omid Saghatchian, Atiyeh Gh. Moghadam, and Ahmad Nickabadi. Cached adaptive token merging: Dynamic token reduction and redundant computation elimination in diffusion model, 2025. 3
- [37] Chitwan Saharia, William Chan, Saurabh Saxena, Lala Li, Jay Whang, Emily L Denton, Kamyar Ghasemipour, Raphael Gontijo Lopes, Burcu Karagol Ayan, Tim Salimans, et al. Photorealistic text-to-image diffusion models with deep language understanding. *Advances in neural information processing systems*, 35:36479–36494, 2022. 6
- [38] Tim Salimans and Jonathan Ho. Progressive distillation for fast sampling of diffusion models. *arXiv preprint arXiv:2202.00512*, 2022. 2
- [39] Tim Salimans, Thomas Mensink, Jonathan Heek, and Emiel Hoogeboom. Multistep distillation of diffusion models via moment matching. *Advances in Neural Information Processing Systems*, 37:36046–36070, 2024. 2
- [40] Pratheba Selvaraju, Tianyu Ding, Tianyi Chen, Ilya Zharkov, and Luming Liang. Fora: Fast-forward caching in diffusion transformer acceleration. *arXiv preprint arXiv:2407.01425*, 2024. 2, 3, 6, 7, 14, 16
- [41] Yuzhang Shang, Zhihang Yuan, Bin Xie, Bingzhe Wu, and Yan Yan. Post-training quantization on diffusion models. In *Proceedings of the IEEE/CVF conference on computer vision and pattern recognition*, pages 1972–1981, 2023. 3
- [42] Andy Shih, Suneel Belkhale, Stefano Ermon, Dorsa Sadigh, and Nima Anari. Parallel sampling of diffusion models. *Advances in Neural Information Processing Systems*, 36, 2024. 3
- [43] Jascha Sohl-Dickstein, Eric Weiss, Niru Maheswaranathan, and Surya Ganguli. Deep unsupervised learning using nonequilibrium thermodynamics. In *International conference on machine learning*, pages 2256–2265. PMLR, 2015. 1
- [44] Jiaming Song, Chenlin Meng, and Stefano Ermon. Denoising diffusion implicit models. *arXiv preprint arXiv:2010.02502*, 2020. 2, 3
- [45] Yang Song and Prafulla Dhariwal. Improved techniques for training consistency models. In *The Twelfth International Conference on Learning Representations*, 2024. 2
- [46] Yang Song and Stefano Ermon. Generative modeling by estimating gradients of the data distribution. *Advances in neural information processing systems*, 32, 2019. 1, 3
- [47] Yang Song, Jascha Sohl-Dickstein, Diederik P Kingma, Abhishek Kumar, Stefano Ermon, and Ben Poole. Score-based generative modeling through stochastic differential equations. In *International Conference on Learning Representations*, 2021. 1, 2, 3
- [48] Yang Song, Prafulla Dhariwal, Mark Chen, and Ilya Sutskever. Consistency models. In *International Conference on Machine Learning*, 2023. 2
- [49] Wenzhang Sun, Qirui Hou, Donglin Di, Jiahui Yang, Yongjia Ma, and Jianxun Cui. Unicp: A unified caching and pruning framework for efficient video generation, 2025. 3, 14
- [50] Zhiwei Tang, Jiasheng Tang, Hao Luo, Fan Wang, and Tsung-Hui Chang. Accelerating parallel sampling of diffusion models. In *Forty-first International Conference on Machine Learning*, 2024. 3
- [51] Wan Team. Wan: Open and advanced large-scale video generative models. 2025. 7, 8
- [52] Jiazheng Xu, Xiao Liu, Yuchen Wu, Yuxuan Tong, Qinkai Li, Ming Ding, Jie Tang, and Yuxiao Dong. ImageReward: Learning and Evaluating Human Preferences for Text-to-Image Generation, 2023. arXiv:2304.05977 [cs]. 6
- [53] Ling Yang, Zhilong Zhang, Yang Song, Shenda Hong, Runsheng Xu, Yue Zhao, Wentao Zhang, Bin Cui, and Ming-Hsuan Yang. Diffusion models: A comprehensive survey of methods and applications. *ACM computing surveys*, 56(4): 1–39, 2023. 1
- [54] Tianwei Yin, Michaël Gharbi, Taesung Park, Richard Zhang, Eli Shechtman, Fredo Durand, and William T. Freeman. Improved distribution matching distillation for fast image synthesis. In *The Thirty-eighth Annual Conference on Neural Information Processing Systems*, 2024. 2
- [55] Tianwei Yin, Michaël Gharbi, Richard Zhang, Eli Shechtman, Fredo Durand, William T Freeman, and Taesung Park.

- One-step diffusion with distribution matching distillation. In *Proceedings of the IEEE/CVF Conference on Computer Vision and Pattern Recognition*, pages 6613–6623, 2024. [2](#)
- [56] Evelyn Zhang, Bang Xiao, Jiayi Tang, Qianli Ma, Chang Zou, Xuefei Ning, Xuming Hu, and Linfeng Zhang. Token pruning for caching better: 9 times acceleration on stable diffusion for free, 2024. [3](#)
- [57] Kaiwen Zheng, Cheng Lu, Jianfei Chen, and Jun Zhu. DPM-solver-v3: Improved diffusion ODE solver with empirical model statistics. In *Thirty-seventh Conference on Neural Information Processing Systems*, 2023. [2](#)
- [58] Zhixin Zheng, Xinyu Wang, Chang Zou, Shaobo Wang, and Linfeng Zhang. Compute only 16 tokens in one timestep: Accelerating Diffusion Transformers with Cluster-Driven Feature Caching. In *Proceedings of the 33rd ACM International Conference on Multimedia (MM '25)*, page to appear, Dublin, Ireland, 2025. ACM. [2](#)
- [59] Haowei Zhu, Dehua Tang, Ji Liu, Mingjie Lu, Jintu Zheng, Jinzhang Peng, Dong Li, Yu Wang, Fan Jiang, Lu Tian, Spandan Tiwari, Ashish Sirasao, Jun-Hai Yong, Bin Wang, and Emad Barsoum. Dip-go: A diffusion pruner via few-step gradient optimization, 2024. [3](#)
- [60] Chang Zou, Evelyn Zhang, Runlin Guo, Haohang Xu, Conghui He, Xuming Hu, and Linfeng Zhang. Accelerating diffusion transformers with dual feature caching, 2024. [2](#)
- [61] Chang Zou, Xuyang Liu, Ting Liu, Siteng Huang, and Linfeng Zhang. Accelerating diffusion transformers with token-wise feature caching. In *Proceedings of the 13th International Conference on Learning Representations (ICLR 2025)*. ICLR, 2025. [2](#), [6](#), [7](#), [14](#), [16](#)

# Adaptive Spectral Feature Forecasting for Diffusion Sampling Acceleration

## Supplementary Material

### A. Proofs

#### A.1. Proof of Theorem 3.1

*Proof.* The proof follows directly from Taylor's theorem with the Lagrange form of the remainder. Let  $f \in \mathcal{F}_{P+1}(L)$ . For any  $\tau_j, \tau_k \in [0, 1]$ , Taylor's theorem states that there exists a  $\xi$  between  $\tau_k$  and  $\tau_j$  such that:

$$f(\tau_j) = \sum_{p=0}^P \frac{f^{(p)}(\tau_k)}{p!} (\tau_j - \tau_k)^p + \frac{f^{(P+1)}(\xi)}{(P+1)!} (\tau_j - \tau_k)^{P+1}.$$

The predictor  $T_P[f](\tau_j)$  is defined as the first term (the Taylor polynomial). Thus, the approximation error is the absolute value of the remainder term:

$$|f(\tau_j) - T_P[f](\tau_j)| = \left| \frac{f^{(P+1)}(\xi)}{(P+1)!} (\tau_j - \tau_k)^{P+1} \right|.$$

Since  $f \in \mathcal{F}_{P+1}(L)$ , we have  $\|f^{(P+1)}\|_\infty \leq L$ , which implies  $|f^{(P+1)}(\xi)| \leq L$ . Substituting the step size  $\tau_j - \tau_k = (j - k)\delta_t$ , we obtain the upper bound:

$$|f(\tau_j) - T_P[f](\tau_j)| \leq \frac{L}{(P+1)!} ((j - k)\delta_t)^{P+1}.$$

To show that this is the supremum (worst-case error), consider the specific function  $f^*(\tau) = \frac{L}{(P+1)!} (\tau - \tau_k)^{P+1}$ . The  $(P+1)$ -th derivative of  $f^*$  is identically  $L$ , so  $f^* \in \mathcal{F}_{P+1}(L)$ . For this function, the derivatives  $f^{*(p)}(\tau_k)$  are 0 for all  $p \leq P$ , meaning  $T_P[f^*](\tau_j) = 0$ . The error is exactly  $|f^*(\tau_j)| = \frac{L}{(P+1)!} ((j - k)\delta_t)^{P+1}$ , which attains the bound.  $\square$

#### A.2. Proof of Theorem 3.2

*Proof.* This result is a standard theorem in approximation theory, often referred to as Bernstein's Theorem for Chebyshev approximation. Recall that any function  $f$  analytic on the Bernstein ellipse  $E_\rho$  can be expanded in a Chebyshev series  $f(\tau) = \sum_{k=0}^{\infty} a_k T_k(\tau)$ . The coefficients  $a_k$  satisfy the geometric decay bound  $|a_k| \leq 2B\rho^{-k}$  for  $k \geq 1$ , where  $B = \sup_{z \in E_\rho} |f(z)|$ .

The truncation error  $f(\tau) - p_M(\tau)$  consists of the tail of the series:

$$f(\tau) - p_M(\tau) = \sum_{k=M+1}^{\infty} a_k T_k(\tau).$$

Taking the infinity norm on  $[-1, 1]$  and using the property that  $|T_k(\tau)| \leq 1$  for  $\tau \in [-1, 1]$ :

$$\|f - p_M\|_\infty \leq \sum_{k=M+1}^{\infty} |a_k| \leq \sum_{k=M+1}^{\infty} 2B\rho^{-k}.$$

The right-hand side is a geometric series with ratio  $\rho^{-1} < 1$ :

$$\sum_{k=M+1}^{\infty} 2B\rho^{-k} = 2B \frac{\rho^{-(M+1)}}{1 - \rho^{-1}} = \frac{2B\rho^{-M}}{\rho - 1}.$$

Thus,  $\|f - p_M\|_\infty \leq \frac{2B}{\rho - 1} \rho^{-M}$ .  $\square$

### A.3. Proof of Theorem 3.3

Let  $h_i(t)$  be the true feature function and  $p_M(t) = \phi(\tau)\mathbf{C}^*$  be its optimal Chebyshev approximation of degree  $M$ , where  $\mathbf{C}^*$  is the vector of ideal Chebyshev coefficients. From Theorem 3.2, we define the truncation error function  $e(t) = h_i(t) - p_M(t)$ , bounded by  $|e(t)| \leq \epsilon_M$ .

We observe data at cached timesteps  $\mathbb{C}_{t_j} = \{(\mathbf{h}_{t_k}, t_k)\}$ . Let  $\mathbf{H} \in \mathbb{R}^K$  be the vector of observed values for channel  $i$  (dropping indices  $t_j$  for simplicity). We can write the observation model as:

$$\mathbf{H} = \Phi \mathbf{C}^* + \mathbf{E},$$

where  $\Phi$  is the design matrix and  $\mathbf{E}$  is the vector of truncation errors at the cached points, with  $\|\mathbf{E}\|_\infty \leq \epsilon_M$ . The fitted coefficients  $\hat{\mathbf{C}}$  are obtained via ridge regression:

$$\hat{\mathbf{C}} = (\Phi^\top \Phi + \lambda \mathbf{I})^{-1} \Phi^\top \mathbf{H}.$$

Substituting  $\mathbf{H}$ :

$$\hat{\mathbf{C}} = (\Phi^\top \Phi + \lambda \mathbf{I})^{-1} \Phi^\top (\Phi \mathbf{C}^* + \mathbf{E}).$$

We want to bound the prediction error at a new time  $t_j$  (with  $\tau_j = g(t_j)$ ). The true value is  $h_i(t_j) = \phi(\tau_j)\mathbf{C}^* + e(t_j)$ , and the prediction is  $\hat{h}_i(t_j) = \phi(\tau_j)\hat{\mathbf{C}}$ . The error is:

$$\hat{h}_i(t_j) - h_i(t_j) = \phi(\tau_j)(\hat{\mathbf{C}} - \mathbf{C}^*) - e(t_j).$$

Let  $\mathbf{A} = \Phi^\top \Phi + \lambda \mathbf{I}$ . Note that  $\mathbf{A}^{-1} \Phi^\top \Phi = \mathbf{I} - \lambda \mathbf{A}^{-1}$ . The coefficient error is:

$$\begin{aligned} \hat{\mathbf{C}} - \mathbf{C}^* &= \mathbf{A}^{-1} \Phi^\top (\Phi \mathbf{C}^* + \mathbf{E}) - \mathbf{C}^* \\ &= (\mathbf{A}^{-1} \Phi^\top \Phi - \mathbf{I}) \mathbf{C}^* + \mathbf{A}^{-1} \Phi^\top \mathbf{E} \\ &= -\lambda \mathbf{A}^{-1} \mathbf{C}^* + \mathbf{A}^{-1} \Phi^\top \mathbf{E}. \end{aligned}$$

Substituting this back into the prediction error:

$$\hat{h}_i(t_j) - h_i(t_j) = \phi(\tau_j) \mathbf{A}^{-1} \Phi^\top \mathbf{E} - \lambda \phi(\tau_j) \mathbf{A}^{-1} \mathbf{C}^* - e(t_j).$$

Using the triangle inequality:

$$|\hat{h}_i - h_i| \leq |\phi(\tau_j) \mathbf{A}^{-1} \Phi^\top \mathbf{E}| + |\lambda \phi(\tau_j) \mathbf{A}^{-1} \mathbf{C}^*| + |e(t_j)|.$$

Now we bound each term.

For the first term, we have  $|\phi \mathbf{A}^{-1} \Phi^\top \mathbf{E}| \leq \|\phi\|_2 \|\mathbf{A}^{-1}\|_2 \|\Phi^\top \mathbf{E}\|_2$ . Since  $|T_m| \leq 1$ , we have  $\|\phi(\tau_j)\|_2 \leq \sqrt{M+1}$ . We also have  $\|\mathbf{A}^{-1}\|_2 \leq \frac{1}{\sigma_{\min}^2(\Phi) + \lambda}$ , and  $\|\Phi^\top \mathbf{E}\|_2 = \|\sum_{k=1}^K \phi(\tau_k)^\top E_k\|_2 \leq \sum_{k=1}^K \|\phi(\tau_k)\|_2 |E_k| \leq K \sqrt{M+1} \epsilon_M$ .

Combining the above, we have  $|\phi \mathbf{A}^{-1} \Phi^\top \mathbf{E}| \leq \frac{(M+1)K}{\sigma_{\min}^2 + \lambda} \epsilon_M$ .

For the second term, we have  $|\lambda \phi \mathbf{A}^{-1} \mathbf{C}^*| \leq \lambda \|\phi\|_2 \|\mathbf{A}^{-1}\|_2 \|\mathbf{C}^*\|_2$ . By the coefficient bound, we get

$$\|\mathbf{C}^*\|_2 \leq \sqrt{\sum_{m=0}^{\infty} 4B^2 \rho^{-2m}} = 2B \sqrt{\frac{1}{1 - \rho^{-2}}}.$$

Combining with the bound in the first term, we have  $|\lambda \phi \mathbf{A}^{-1} \mathbf{C}^*| \leq \frac{\lambda \sqrt{M+1}}{\sigma_{\min}^2 + \lambda} \frac{2B}{\sqrt{1 - \rho^{-2}}}$ .

For the third term,  $|e(t_j)| \leq \epsilon_M$ .

Therefore, combining the bound for the three terms above gives the final bound:

$$|h_i(t_j) - \hat{h}_i(t_j)| \leq \epsilon_M \left( 1 + \frac{(M+1)K}{\sigma_{\min}^2 + \lambda} \right) + \frac{\lambda \sqrt{M+1}}{\sigma_{\min}^2 + \lambda} \frac{2B}{\sqrt{1 - \rho^{-2}}}.$$

## B. More Method Details

### B.1. Adaptive Scheduling

Most previous works [22, 40, 61] on diffusion caching employ a uniform scheduling in selecting  $\mathbb{U}$  *i.e.*, the set of timesteps to perform full network evaluation. For this strategy, a full network evaluation is performed every fixed interval of length  $\mathcal{N} \in \mathbb{N}^+$ . Under our framework, this corresponds to  $\mathbb{U}_{\text{uniform}} = \{1\} \cup \{\tau_j : j = r\mathcal{N}, r \in \mathbb{N}^+, 1 \leq j \leq N\}$ , where  $N = 50$  is the total number of discretization timesteps. However, this scheduling does not account for the fact that errors made in early diffusion steps accumulate and disproportionately affect later steps, eventually degrading the final output more significantly.

Other works [21, 26, 30, 49] attempt to address this by adaptively adjusting the scheduling  $\mathbb{U}$ , but their methods typically require tracking inference time metrics, which introduces additional computation overheads. In contrast, we propose a simple, precomputed adaptive scheduling that progressively increases the interval length between adjacent timesteps, formulated as:

$$\mathbb{U} = \{\tau_j : j = \lfloor \alpha \frac{r(r+1)}{2} \rfloor, r \in \mathbb{N}^+, 1 \leq j \leq N\},$$

where  $\alpha \geq 0$  characterizes the *rate of increase* of the interval  $\tau_j - \tau_k$  between adjacent timesteps  $j$  and  $k$ .

**Unified parameterization.** Besides this progressively increasing recomputation intervals, our actual implementation has two additional components: the initial interval size  $\mathcal{N}$  and the number of warm-up steps  $\mathcal{W}$ , which are *directly inherited* from the original setup in TaylorSeer [22]. The initial interval size  $\mathcal{N}$  determines the length of the first interval, from which subsequent intervals grow. The warm-up step  $\mathcal{W}$  corresponds to the length of the initial phase during which full network evaluations are computed at every step, before the caching and forecasting procedure begins. The detailed formulation of *Spectrum*'s adaptive scheduling incorporated with these two hyperparameters is as follows:

$$\mathbb{U} = \{\tau_j : j \in \mathbb{N}^+, 1 \leq j \leq \mathcal{W}\} \cup \left\{ \tau_j : j = \mathcal{W} + \left\lfloor (r+1)\mathcal{N} + \alpha \frac{r(r+1)}{2} \right\rfloor, r \in \mathbb{N}, 1 \leq j \leq N \right\}.$$

Therefore, the uniform scheduling  $\mathbb{U}_{\text{uniform}}$  in previous works can be exactly recovered by setting  $\alpha = 0.0$ .

Under this unified parameterization, we provide detailed specifications of the baselines, which are parameterized by  $\mathcal{N}$  and  $\mathcal{W}$ , and *Spectrum*, which is additionally parameterized by  $\alpha$ , in Table 6. For clarity, we also include their corresponding number of network evaluations (NFE), which is closely related to their actual wall clock time reported in the main tables.

## C. More Experiment Details

### C.1. Model Settings

**Text-to-image.** We employ FLUX.1-dev<sup>3</sup> and Stable Diffusion 3.5-Large<sup>4</sup> for text-to-image generation. For the main experiments, we generate images with  $1024 \times 1024$  resolution. We apply the default guidance scale, which is 3.5 for FLUX and 7.0 for Stable Diffusion 3.5-Large.

**Text-to-video.** We adopt Wan2.1-14B<sup>5</sup> and HunyuanVideo<sup>6</sup> for text-to-video generation. We generate 480p videos with 81 frames following the prompt suite in VBench [11] and strictly follow the benchmark protocol of VBench to evaluate the quality metrics and VBench Quality Score. Following convention, we apply a guidance scale of 5.0 for Wan2.1-14B and 6.0 for HunyuanVideo throughout all experiments.

### C.2. Baseline Settings

For the baselines that employ a uniform activation scheduling (FORA, ToCa, and TaylorSeer), we set interval size  $\mathcal{N}$  to be 4 in the slow acceleration setting and 6 in the high acceleration setting. We set  $\mathcal{W} = 1$  for FORA,  $R = 90\%$ ,  $\mathcal{W} = 3$  for ToCa, and  $\mathcal{W} = 5$  for TaylorSeer to match the evaluation setting in Liu et al. [22]. TeaCache employs a non-deterministic scheduling that may vary across different runs, but we found that setting the caching threshold  $\delta$  to 0.2 and 0.8 results in similar acceleration rates.

For *Spectrum*, we use the same number of warm-up steps ( $\mathcal{W} = 5$ ) as TaylorSeer and set  $\mathcal{N} = 2$  for the settings that use the adaptive activation scheduling. We set  $\alpha = 0.75$  and  $\alpha = 3.0$ , respectively, for the slow and high acceleration settings.

<sup>3</sup>black-forest-labs/FLUX.1-dev

<sup>4</sup>stabilityai/stable-diffusion-3.5-large

<sup>5</sup>Wan-AI/Wan2.1-T2V-14B

<sup>6</sup>hunyuanvideo-community/HunyuanVideo

Table 6. Detailed specification on the scheduler and the total number of network evaluations (NFE) for all methods. “Reference” refers to the tables in the main paper where the corresponding method was mentioned.

	Reference	$\mathcal{N}$	$\mathcal{W}$	$\alpha$	NFE
FORA ( $\mathcal{N} = 4$ )	Table 1, 2	4	1	0.0	13
ToCa ( $\mathcal{N} = 4$ )	Table 1, 2	4	3	0.0	14
TaylorSeer ( $\mathcal{N} = 4$ )	Table 1, 2	4	5	0.0	16
<i>Spectrum</i> ( $\alpha = 0.75$ )	Table 1, 2	2	5	0.75	14
FORA ( $\mathcal{N} = 6$ )	Table 1, 2	6	1	0.0	9
ToCa ( $\mathcal{N} = 6$ )	Table 1, 2	6	3	0.0	10
TaylorSeer ( $\mathcal{N} = 6$ )	Table 1, 2	6	5	0.0	12
<i>Spectrum</i> ( $\alpha = 3.0$ )	Table 1, 2	2	5	3.0	10
TaylorSeer ( $\mathcal{N} = 8$ )	Table 3	8	5	0.0	10
TaylorSeer ( $\alpha = 3.0$ )	Table 3	2	5	3.0	10
<i>Spectrum</i> ( $\mathcal{N} = 8$ )	Table 3	8	5	0.0	10
<i>Spectrum</i> ( $\alpha = 3.0$ )	Table 3	2	5	3.0	10

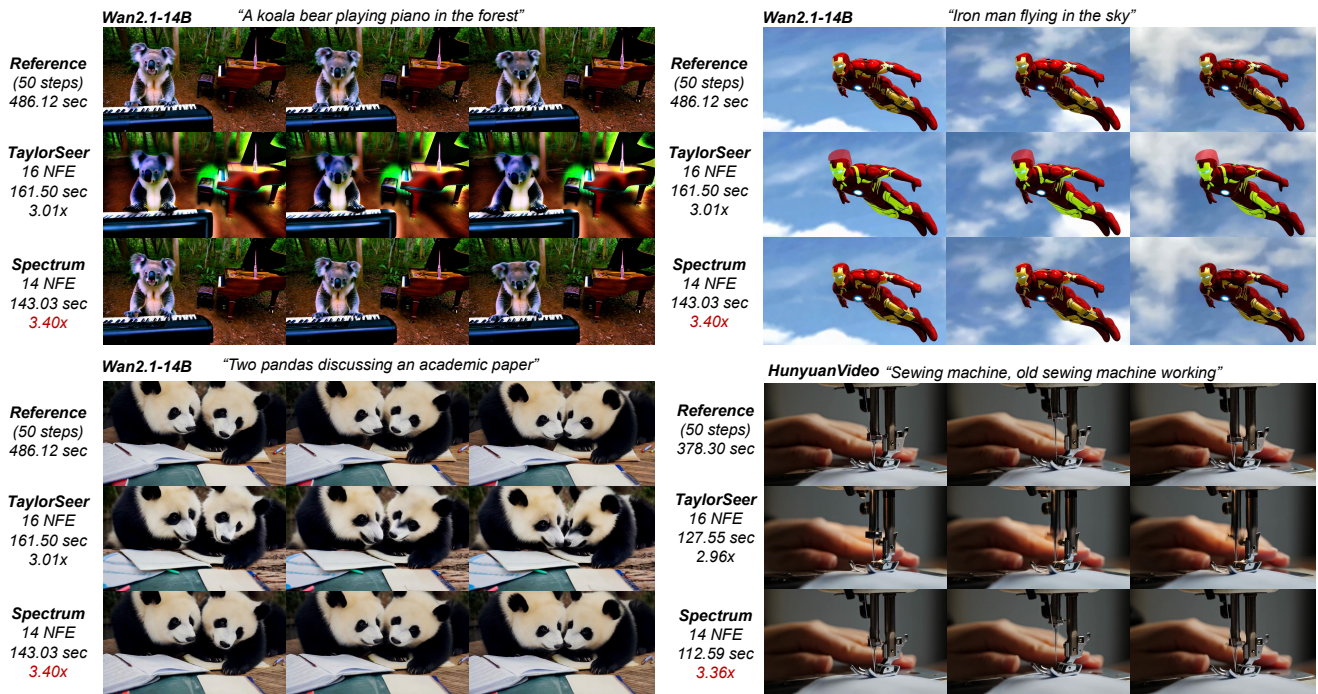


Figure 7. Additional qualitative comparison on text-to-video generation using Wan2.1-14B and HunyuanVideo.

### C.3. Ablation Study Settings

We conduct the ablation on the adaptive activation scheduling in the high-speed up setting to better visualize its impact. To ensure a fair comparison under the same computation budget, we set the Taylor polynomial method’s interval size to  $\mathcal{N} = 8$ , which lets it consume the same number of network evaluations (NFE) as *Spectrum* with  $\alpha = 3.0$ . We conducted the ablation study on the effect of last-block forecasting at the preliminary stage of our project, so we used the uniform activation scheduling with  $N = 8$  for both the Taylor method and *Spectrum*. We use adaptive scheduling for the ablation study on the regularization weight  $\lambda$  and the degree of the Chebyshev polynomial  $M$ . The 5 different acceleration ratios in Figs. 5 and 6 correspond to the  $\alpha$  values [0.2, 0.4, 0.75, 1.5, 3.0], which incur the following NFEs [20, 17, 14, 12, 10].

Table 7. Benchmark results of **text-to-image generation** on COCO2017 [19] using FLUX.1. We use 50 steps as the reference (†). Our *Spectrum* achieves higher speedup while maintaining better sample quality.

	FLUX.1 [17]						
	Acceleration		Quality			Image Reward†	CLIP†
	Latency(s)↓	Speedup†	PSNR†	SSIM†	LPIPS↓		
50 steps†	26.46	1.00	-	-	-	1.13	25.92
FORA ( $\mathcal{N} = 6$ ) [40]	6.37	4.16	13.94	0.604	0.523	1.04	<b>26.10</b>
ToCa ( $\mathcal{N} = 6, \mathcal{R} = 0.9$ ) [61]	13.51	1.96	16.14	0.652	0.462	1.10	<b>26.10</b>
TeaCache ( $\delta = 0.8$ ) [21]	6.73	3.94	16.07	0.664	0.436	1.03	25.88
TaylorSeer ( $\mathcal{N} = 6, \mathcal{O} = 1$ ) [22]	6.52	4.06	19.92	0.782	0.297	1.10	25.98
<i>Spectrum</i> ( $\alpha = 3.0$ )	<b>5.58</b>	<b>4.75</b>	<b>22.29</b>	<b>0.811</b>	<b>0.288</b>	<b>1.11</b>	25.95



Figure 8. Qualitative comparison on text-to-image generation using Stable Diffusion 3.5-Large

## D. More Results

**Evaluation on COCO2017 captions dataset.** We provide additional results on the COCO2017 captions dataset [19] using FLUX.1 in Table 7. *Spectrum* consistently exhibits exceptional performance on the new set of prompts.

**More qualitative results.** We provide additional qualitative comparisons on text-to-image generation with FLUX.1 in Fig. 9

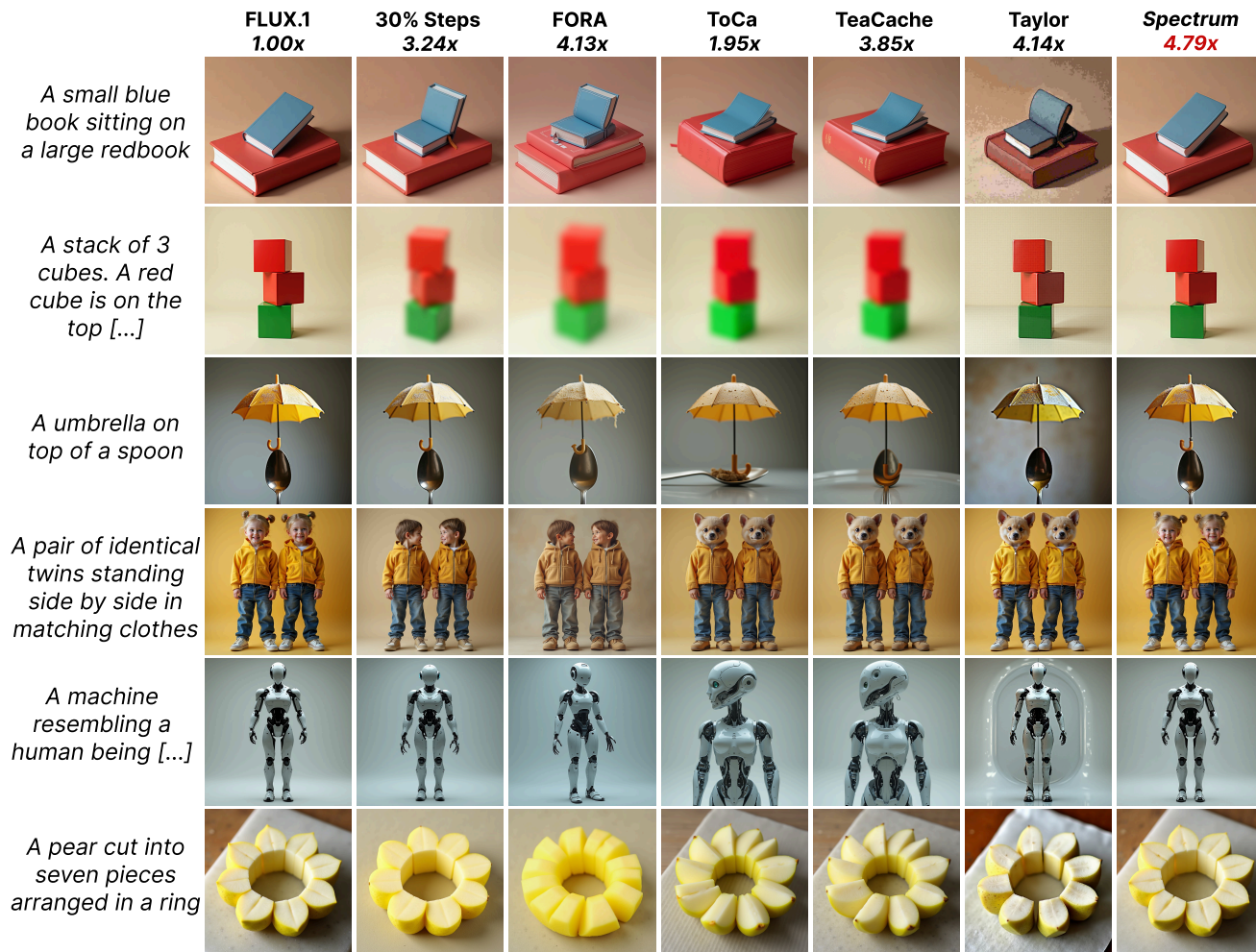


Figure 9. Additional qualitative comparison on text-to-image generation using FLUX.1.

Table 8. RMSE between the predicted latent features and oracle.

	Diffusion step	10	20	30	40	50
Hunyuan	TaylorSeer	0.0047	0.0102	0.0206	0.0467	0.1562
	Spectrum	0.0021	0.0046	0.0081	0.0182	0.0818

	Taylor	Spectrum
PNSR↑	21.87	24.95
SSIM↑	0.768	0.793
LPIPS↓	0.271	0.253
Speedup↑	2.6×	2.8×



50 steps



Spectrum



Taylor

Figure 10. Additional results on SDXL (U-Net architecture).

and with Stable Diffusion 3.5-Large in Fig. 8. We also provide more qualitative comparisons on text-to-image generation with Wan2.1-14B and HunyuanVideo in Fig. 7. We offer more visualizations of the generated video samples with *Spectrum* using HunyuanVideo in Fig. 11.

**More latent feature results.** We provide RMSE on latent features on HunyuanVideo in Table 8.

**Generalization to U-Net architecture.** We additionally investigate the efficacy of *Spectrum* on SDXL with U-Net architecture. Results are summarized in Fig. 10, which shows that *Spectrum* remains highly effective on SDXL, outperforming TaylorSeer by a significant margin.



*A massive, ancient space whale, [...] breaching from a swirling, purple gaseous nebula. [...] in slow motion, [...] catching the light of a distant supernova.*



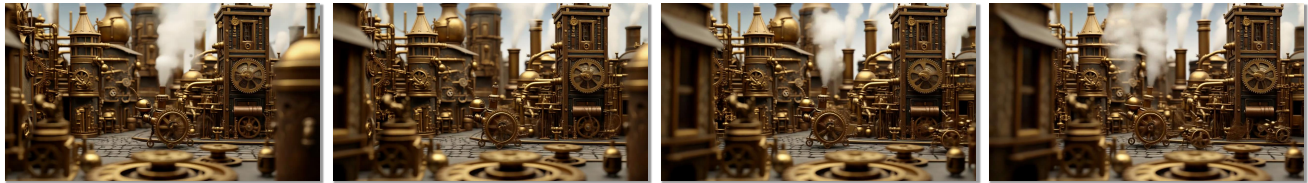
*A chef in a bustling kitchen [...] The chef chops and plates food with incredible speed, while flames erupt from pans, steam billows from pots [...]*



*An aerial shot of a vast city at night, but each individual light source [...] pulses and shifts through a full spectrum of colors [...]*



*A hallway made entirely of mirrors, reflecting a person walking, but the reflections are out of sync and show different versions of the person*



*A macro dolly-in shot of a complex, clockwork city, tiny brass gears turning and steam escaping from miniature pipes as miniature automatons walk the streets*



*A person walking down a hallway, but with every step, the walls, floor, and ceiling fracture into geometric shards that swirl around them [...]*



*A drone shot flying straight up the face of a colossal, thundering waterfall in a lush, tropical gorge [...] while a rainbow forms in the drifting mist*

Figure 11. More **text-to-video generation samples** on HunyuanVideo with *Spectrum*. Samples were generated using only **14 network evaluations**, leading to a significant speedup of  $3.5\times$  without quality degradation.